Shaping the terahertz sound propagation in water under highly directional confinement

Alessio De Francesco, Luisa Scaccia, Ferdinando Formisano, Marco Maccarini, Francesco De Luca, Alexandra Parmentier, Ahmet Alatas, Alexey Suvorov, Yong Q. Cai, Ruipeng Li, and Alessandro Cunsolo

Phys. Rev. B **101**, 054306 — Published 25 February 2020

DOI: 10.1103/PhysRevB.101.054306

Shaping the Terahertz Sound Propagation in Water Under Highly-Directional Confinement

Alessio De Francesco,[1] Luisa Scaccia,[2] Ferdinando Formisano,[1] Marco Maccarini,[3] Francesco De Luca,[4] Alexandra Parmentier,[5] Ahmet Alatas,[6] Alexey Suvorov,[7] Yong Q. Cai,[7] Ruipeng Li,[7] and Alessandro Cunsolo[7*]

1. Consiglio Nazionale delle Ricerche, Istituto Officina dei Materiali c/o OGG and Institut Laue Langevin, 71 avenue des Martyrs, 38042 Grenoble, France.

2. Dipartimento di Economia e Diritto, Università di Macerata, Via Crescimbeni 20, 62100 Macerata, Italy.

3. Université Grenoble-Alpes - Laboratoire TIMC/IMAG (UMR CNRS 5525), Pavillon Taillefer, Domaine de la Merci, 38700 La Tronche, France.

4. Dipartimento di Fisica, Sapienza Università di Roma, P.le A. Moro, 2, I-00185 Rome, Italy.

5. INFN - Division of Roma Tor Vergata, V. della Ricerca Scientifica 1, 00133, Rome, Italy.

6. Advanced Photon Source, Argonne National Laboratory, Argonne, Illinois 60439, USA.

7. National Synchrotron Light Source II, Brookhaven National Laboratory, Upton, NY 11973, USA.

*Corresponding Author, e-mail: acunsolo@bnl.gov

Keywords: Inelastic X-ray Scattering, Carbon Nanotubes, Phonon propagations, Reversible Jump Markov Chain Monte Carlo, Bayesian analysis.

Abstract

We consider here the possibility of shaping the high-frequency acoustic propagation in a liquid upon directional confinement. This hypothesis is investigated by Inelastic X-ray Scattering measurements on water confined in aligned multi-walled carbon nanotubes, in which the momentum transfer was either parallel or orthogonal to the confinement axis. The comparison between the spectra measured in these two scattering geometries highlights the anisotropic nature of the dynamic response of directionally confined water, thus potentially inspiring new pathways to shape high-frequency sound propagation in isotropic systems. Finally, a Bayesian analysis of measured spectra unravels close similarities in the phonon dispersions of multiwalled nanotubes and graphite.

INTRODUCTION

The control of acoustic propagation through composite materials is one of the new research frontiers of condensed matter physics, whose relevance has been fully recognized.[1] The advancement of this research field has prompted a growing interest in complex mesoscale structures displaying non-trivial phononic properties at terahertz frequencies. This increasing attention owes to the ability of terahertz phonon propagation to convey heat flow through insulators, which makes it possible to implement heat management based on the structural design.

When dealing with an isotropic system such as a fluid, the shaping of acoustic properties is not straightforward, as density waves in these systems are much more short-lived than their counterparts in crystalline materials and do not have preferential propagation directions. The breaking of the acoustic isotropy of the fluid requires, for instance, its containment inside highly directional cavities. Carbon nanotubes (CNTs) are ideal candidates to fulfil this duty, as they act as quasi-unidimensional flow channels for the liquid trapped therein.[2] In particular, confinement in CNTs is known to drastically modify the physical properties of embedded water [3] including its dipolar configuration [4,5] and orientational relaxation.[6] Furthermore, when trapped inside CNTs, water exhibits a non-trivial temperature evolution, characterized by multiple transitions, such as a fragile-to-strong crossover of the diffusion coefficient,[7] an anomalously soft phonon response in the solid phase,[8] and several changes between distinct relaxational regimes.[9]

It is well-established that unidimensional confinement reduces the overall number of hydrogen bonds (HBs) of water aligning them preferentially along the CNTs axes,[10] and favors the tendency of water to get arranged in concentric layers inside the CNT interiors,[8,11] in which water molecules tend to group in hydrogen-bonded chains. Also, the diffusive dynamics of water is profoundly affected by this type of confinement,[12,13] and, again, it becomes preferentially directed along the CNT longitudinal axis.

Although transport and structural properties of axially confined water have been the focus of intensive scrutiny, no comparable understanding has been thus far reached for the phonon-like, dynamics. This circumstance partly owes to the absence of large-scale alignment in CNT samples - typically available only in powder-like aggregates - which prevents a proper disentanglement of CNT phonon excitations propagating either axially or radially respect to CNT axes.

On a general ground, water seems an ideally-suited candidate as a confined liquid, partly due to the comprehensive investigations of its bulk properties, which provide a valuable reference to compare to. Furthermore, the spectrum of bulk water is dominated by collective modes with both transverse and longitudinal polarizations,[14-17] respectively connected to the intermolecular HB bending and stretching.[18] The close link between the propagation of acoustic modes and HB dynamics, combined with the ability of nanotube confinement to axially "align" water HBs, may have far-reaching implications. For instance, it may suggest that, under such confinement, not only the structure, but also the dynamics becomes anisotropic and preferentially axial, thus opening unexplored avenues in the domain of THz acoustic manipulation.

Overall, the possibility that the axial alignment of HBs upon highly directional confinement may cause an "isotropy breach" of sound propagation, remains an intriguing hypothesis, yet still in demand for dedicated investigations.

To clarify the above points, it would be helpful to assign a macroscopic axial symmetry to the confinement environment by considering, for instance, aligned CNTs (aCNTs) "forest-grown" orthogonally to a common substrate.[19]

Spectroscopic techniques, such as Inelastic X-ray, IXS,[20] and Neutron Scattering, INS,[21] are ideally suited to characterize terahertz acoustic propagation on such systems. First, they can be used to stimulate phonon-like excitations with nanometer wavelengths, whose propagation is likely to be impacted by the mesoscale structure of aCNT arrays. Second, they provide direct access to the spectrum of density fluctuations $S(\boldsymbol{Q},E)$, which is a single-valued function of the energy, E, and momentum, $\boldsymbol{Q}$, transferred from the probe to the sample. This calls for parallel spectroscopic measurements in which the scattered intensity is collected with the momentum

transfer aligned either axially or in the radial plane of the target aCNTs. These two scattering geometries will be hereafter referred to as $\mathbf{Q}_{\parallel}$ and, $\mathbf{Q}_{\perp}$ respectively (see Figure 1A, B).

In the present measurements, the scattering plane, i.e. the plane containing both the incident and scattered beam, is horizontal, therefore the $\mathbf{Q}_{\perp}$ and $\mathbf{Q}_{\parallel}$ geometries correspond to a vertical and horizontal orientation of the aCNT axis, respectively.

Performing measurements in $\mathbf{Q}_{\parallel}$ geometry (Figure 1B) poses practical challenges, as in this scattering configuration the incident beam directly crosses the substrate, which may provide a non-negligible contribution to the spectral density, thus hampering the reliable determination of the actual sample signal. To circumvent this problem, we opted instead for a grazing incident geometry, as shown in Figure 1C. Notice that, for small scattering angles, in this geometry the momentum is substantially transferred along the nanotube axis as well.

As mentioned, one of the primary motivations of the present work was to assess possible dynamic anisotropies in the spectrum of directionally confined water, based on the comparison between $\mathbf{Q}_{\perp}$ and $\mathbf{Q}_{\parallel}$ IXS spectra from hydrated and dry multi-walled CNTs (MWCNTs). Those considered here are aligned MWCNTs (aMWCNTs) "forest grown" on a Si substrate and having about 1 mm length, an external diameter of 10 nm and a core diameter of about 5 nm.

The main difficulty to be faced when hydrating forest-grown CNTs is that they are closed on both ends, being capped on the top and attached to the substrate on the bottom. Therefore, they can hardly host hydration water in their interior unless intentionally uncapped, which is not advisable if the mutual nanotube alignment has to be preserved.

Being individual CNTs impenetrable to water, *a priori* hydrated CNT forests can only absorb interstitial water - or, possibly, bulk water - in their inter-CNT voids.[22] However, the last possibility seems against current experimental evidence, as no relic of either Bragg spots or ice phonon peaks can be respectively found in diffraction and inelastic measurements at the temperature T = 100 K displayed in the Supplemental Material [23] (see also references [1,2] therein).

Conversely, the presence – or, at least, the spectral dominance - of interstitial water is unambiguously unveiled by the circumstance that spectral profiles measured on wet samples in $\mathbf{Q}_\perp$ geometry are substantially different from the resolution function and the dry matrix spectrum, and, most importantly, from the unmistakable spectral shape of bulk water.[15-18] It is worth noticing that interstitial water is subjected to highly directional confinement, as it remains preferentially trapped within the nanotube bundles of the aMWCNT matrix. Indeed, upon wetting, carbon nanotubes in a bundle tend to cluster under the effect of capillary forces, and interstitial water remains trapped in the axial cavities formed by three neighboring carbon nanotubes at contact. It can be estimated that these interstices have length comparable with that of aMWCNTs (about 1 mm), and their nearly triangular cross-section has an area of about 4 nm^2, matching that of a 2.24 nm diameter nanotube. Although it is unclear how water distributes inside this highly directional cavity, it would become very tightly confined in the three contact corners between adjacent aMWCNTs.

The arguments above made us confident that the relevant contribution to the measured IXS spectra comes uniquely from interstitial water and the carbon matrix. To better disentangle these two spectral contributions, we performed measurements on both hydrated and dry samples. This also enabled us to characterize the phonon dispersion in bare aMWCNTs, which has its own

interest, considering the lack of related information in the literature. Again, a reliable interpretation of these scattering results critically depends on the mutual alignment and orientation of the CNT array.

The case of MWCNTs considered here can be directly related to the one of graphite. Indeed, an MWCNT, at least conceptually, can be generated by rolling up a few graphene layers to form an ensemble of nested coaxial cylinders. Aside of theoretical computations,[24] the phonon dispersion of (single- or multi-walled) carbon nanotubes is thus usually derived from measurements performed on graphite,[25,26] via the zone-folding method, instead of being measured on actual CNT samples. Elucidating the analogies/differences with respect to the known case of graphite was amongst the initial objectives of this study.

Overall, experimental results presented here show that IXS spectra of hydrated aMWCNTs measured in either $\mathbf{Q}_{\perp}$ or $\mathbf{Q}_{\parallel}$ geometry have a markedly different shape, which highlights the anisotropic nature of the dynamic response of these samples. Also, the comparison with corresponding dry sample spectra suggests that this anisotropy is due to the trapped interstitial water.

The IXS spectral shape was modelled following a Bayesian inferential method,[27] as implemented using a Monte Carlo Markov Chain (MCMC) algorithm integrated with a Reversible Jump (RJ) option.[28] Such an approach enables to test various hypotheses on the number of dominant spectral modes, as required for a proper interpretation of the measured spectral shape.

As a result, this analysis brings about the determination of three sound dispersion branches. The lowest-energy one relates to a mode dominating the $\mathbf{Q}_{\perp}$ spectrum of the hydrated sample, which

we assign to a vibrational mode arising from the degrees of freedom of interstitial water molecules, and likely connected with the transverse acoustic mode of bulk water. The two remaining dispersive branches are consistent with those experimentally determined in graphite, and are thus attributed to phonon modes of the aMWCNTs matrix.

EXPERIMENTAL DETAILS

The measurements have been carried out using the high-resolution spectrometer at the beamline 3 ID of the Advanced Photon Source at Argonne National Laboratory [29,30] and the newly developed beamline 10ID of the National Synchrotron Light Source-II at Brookhaven National Laboratory.[31] The spectrometers were operated with a resolution width of about 2 meV, and had complementary strengths, that is, a high scattering count rate (Sector 3) and a high spectral contrast ensured by the nearly Gaussian resolution function (10ID). The resolution profile was measured by collecting the scattering signal from a plexiglas sample at a Q value corresponding to the position of its first sharp diffraction peak, where the sample becomes an almost elastic scatterer.

Furthermore, the better Q-resolution of the 10ID measurement enables to perform IXS measurements down to smaller Q values, while conversely, the slower Q decay of scattering intensity made Sector 30 better suited for high-Q measurements.

The incident beam energies were 23.7 keV and 9.13 keV for Sector 3 and 10ID spectrometers, respectively. In both instruments, the energy analysis was performed by rocking the crystals of the monochromator unit, while keeping the analyzers fixed. Such a scan was either implemented through the temperature variation of the active crystal (Sector 3) or by the simultaneous rocking of two crystal pairs arranged in the so-called four-bounce design [32] (10ID). In both instruments,

analyzer units are mounted at the extreme of a spectrometer arm rotating in the horizontal plane and either consisted on four spherical "mosaic" Si analyzers (Sector 3), or a single analyzer unit based on a Collimator-Dispersive-Wavelength selector (CDW) crystal optical design and coupled with an upstream collimating mirror enhancing its angular acceptance (10ID).

For the various sample hydration levels and scattering geometries, IXS spectra were collected at slightly different *Q*-intervals that spanned the 2 ÷ 15.23 nm^{-1} interval, including the first (pseudo) Brillouin zone of (water) graphite, while *E*-scans covered different portions of the -30 meV-30 meV window.

Notice that in both instruments the analyzers are mounted on the outermost side of the spectrometer arm, whose rotation in the horizontal plane determines the *Q* value intercepted by each analyzer. The shape of the energy resolution profile slightly varies for each of these analyzers, which explain why spectra measured at the same *Q* values have slightly different resolution profiles (see, *e.g.*, Figure 3).

The GIWAXS measurements were performed at 11BM Complex Materials Scattering (CMS) beamline at National Synchrotron Light Source II (NSLS-II), Brookhaven National Laboratory. The monochromatic 0.0918 nm wavelength X-Ray beam shines on the thin film sample with the grazing incident angle of 0.12^{o}. An in-vacuum CCD detector (Photonic Science) was placed 229 mm away from the sample for data collection. The exposure time was 30 s for all samples. Data analysis was carried out using the SciAnalysis package (code is available on the site https://github.com/CFN-softbio/SciAnalysis).

The hydration of the a-CNT array was performed by exposition of each sample to steam vapors in an autoclave, according to a protocol succinctly described in Ref. [33].

The IXS measurements at 10ID beamline of NSLS-II on wet and dry samples were executed with the sample in air, and so were all GIWAXS measurements. The IXS and diffraction measurements at Sector 3 (APS) were executed both at ambient and low temperature (100 K), thus requiring the use of a cryostat. In these measurements the sample was enclosed in a vacuum-sealed Be dome filled with an atmosphere of N_2 gas. This expedient was adopted to keep hydration water from being sucked away by the cryostat vacuum, as well as to prevent the formation of bulk ice, typically occurring in low-temperature measurements with the sample in air. Finally, further details on the sample are provided in the Supplemental Material (see also references [3,4] therein).

DISCUSSION

The $\mathbf{Q}_\perp$ and $\mathbf{Q}_\parallel$ IXS spectra measured on the hydrated and the dry samples at Q = 11.95 nm^{-1} are reported in Figure 2 after normalization to the $\omega = 0$ maximum, and compared therein with the corresponding resolution spectra normalized in the same fashion. From the comparisons in the plots it emerges that:

1) **Hydrated sample:** the $\mathbf{Q}_\perp$ spectrum of the hydrated sample is substantially different from its $\mathbf{Q}_\parallel$ counterpart: while the former has low-energy wings substantially broader than the resolution profile, the latter only displays vague reminiscences of inelastic features, which, if present at all, are located at ~ 10 meV at this Q value. The difference between the signals measured in the two geometries emphasizes the anisotropic character of the probed dynamic response.

2) **Dry sample**: The dry sample spectrum mainly coincides with the resolution profile in the $\mathbf{Q}_{\perp}$ case, while the limited statistical accuracy prevents any firm conclusion on the $\mathbf{Q}_{\parallel}$ measurement from a mere visual inspection.

Overall, the $\mathbf{Q}_{\parallel}$ spectrum from the hydrated sample in Figure 2 stands out for the absence of the distinctive inelastic excitations, which are known to dominate the spectrum of bulk water.

To gain further insight into the measured spectral shapes and fully interpret all spectral features observed, we performed a lineshape modelling of $\mathbf{Q}_{\parallel}$ and $\mathbf{Q}_{\perp}$ spectra of both hydrated and dry samples. The analysis was based on a Bayesian inferential method,[27] similar to the one recently adopted to interpret Brillouin INS results on liquid metals,[34] and IXS ones on a suspension of gold nanoparticles.[35] This method ultimately assesses, on solid probabilistic ground, the number of modes most likely to appear in the dynamic structure factor *S(Q,E)* based on the set of experimental measures performed. As mentioned in the Introduction, this inferential method is implemented through a Monte Carlo Markov Chain (MCMC) algorithm integrated with a Reversible Jump (RJ) option [28] and described in further detail elsewhere.[34] Here we only focus on the relevant steps of the data analysis performed.

The first of such steps is the identification of the best-suited lineshape model. In the literature, models for the spectral shape from liquid or glassy samples are often derived in the framework of the so-called Mori-Zwanzig formalism,[36,37] while adopting appropriate assumptions for the time decay of the memory function. However, the spectrum of a hybrid (solid-liquid) system, like an array of hydrated CNTs, is expectedly an unknown combination of solid-like and liquid-like spectral features, which, given the lack of rigorous theories, is here described by the following simplified model:

$$\tilde{S}(Q,E) = A_e(Q)\delta(E) + [n(E)+1]\sum_{j=1}^{k}\frac{2}{\pi}\frac{A_j(Q)\Omega_j^2(Q)\Gamma_j(Q)}{\left[E^2-\Omega_j^2(Q)\right]^2+4\left[\Gamma_j(Q)E\right]^2} \quad (1)$$

where E is the energy transferred from the X-ray photon to the target sample; $\delta(E)$ is the elastic response of the system modulated by a Q-dependent scale factor $A_e(Q)$; $n(E)+1$ is the Bose thermal factor accounting for the detailed balance condition with $n(E) = (exp(E/k_BT)-1)^{-1}$; finally, the model contains a sum of k Damped Harmonic Oscillator (DHO) profiles accounting for purely inelastic contributions to the scattered signal, the j*th* of them being characterized by energy $\Omega_j(Q)$, damping $\Gamma_j(Q)$ and amplitude $A_j(Q)$. We stress here that the number k of purely inelastic modes is treated as a model parameter itself and, within the used Bayesian approach,[27] this implies that its posterior distribution can be obtained along with those of all the other model parameters. As discussed elsewhere,[34] the best fit lineshape is eventually determined using the optimal parameter values, which coincide with the averages or the most probable values, *i.e.* the modes, of the corresponding posterior density distribution.

The most visited model option corresponds to either k = 1 (one DHO term) or k = 2 (two DHO terms), depending on sample, scattering geometry and Q range. An example of the outcome of this Bayesian inference method is provided in Figure S4 of the Supplemental Material.

It is also worth recalling that, in order to fit the measured spectra, the model function of Equation (1) needs to be convoluted with the instrument resolution function and the result assumed to seat on the top of a linear background noise described by two parameters, β_0 and β_1. In summary the model function has the following general form:

$$S(Q,E) = \tilde{S}(Q,E) \otimes R_{exp}(Q,E) + (\beta_0 + \beta_1 E)$$

where $R_{exp}(Q,E)$ is the measured resolution, while the optimized spectral background is substantially flat, i.e. with $\beta_1 = 0$.

The $\mathbf{Q}_\perp$ and $\mathbf{Q}_\parallel$ spectra of the hydrated aMWCNT array are displayed in Figure 3 as measured at three representative Q values along with best-fitting model lineshapes and partial - elastic and inelastic - contributions.

Again, the comparison between best-fit $\mathbf{Q}_\perp$ and $\mathbf{Q}_\parallel$ lineshapes emphasizes the pronounced anisotropy of the dynamic response of the hydrated sample under highly-directional confinement. For both geometries, the most probable model includes a central elastic δ(E) component and a single inelastic DHO term. When comparing $\mathbf{Q}_\perp$ and $\mathbf{Q}_\parallel$ spectra to each other, it can be readily noticed that, in the former case, the DHO peaks (olive line) emerge at lower energies, and have a much stronger relative intensity and a milder Q-dispersion. Indeed, this trend stresses the anisotropic character of the spectral response of the hydrated sample.

As it partially emerges from the plot in Figure 3, the Bayesian analysis also highlights the presence of additional features in the $\mathbf{Q}_\perp$ spectra from the hydrated sample. Namely:

i) an additional inelastic DHO term for $Q < 9$ nm^{-1} (see blue dashed line in the left upper panel of Figure 4). Hints on the presence of this excitation were also found at larger Q values, but they did not correspond to the most probable option, and consequently, this additional high DHO term is not included in the corresponding plot.

ii) an additional inelastic DHO term (magenta line) at the highest Q (> 13 nm^{-1}). In this case, the DHO term is either overdamped ($\Omega < \Gamma$) or has both Ω and Γ much smaller than the resolution spectrum, appearing in either case as a resolution-broadened quasielastic peak (see lowest left panel). We conclude that, at these Q values, a single elastic peak cannot fully account for the quasielastic part of $\mathbf{Q}_\perp$ spectra, possibly owing to the onset of a structural relaxation analogous to the one thoroughly investigated in bulk water,[38,39] which, in principle, should have been explicitly accounted for by the model. A detailed characterization of these viscoelastic lineshape effects will be tackled in a forthcoming paper, as the present solely focuses on the inelastic part of the spectrum, and, more specifically on the influence of highly directional confinement on the acoustic modes of water. For this reason, we decided not to include an additional Lorentzian term to account for the observed quasielastic broadening, using instead for this scope one of the DHO terms included in the model. Indeed, DHO profiles represent a more flexible and "agnostic" model option, which can adapt well to approximate either a low-frequency propagating mode (underdamped DHO) or a non-propagating one (overdamped DHO). Conversely, the use of a Lorentzian term would have externally biased the interpretation of the quasielastic intensity, arbitrarily assigning it to a non-propagating (i.e. diffusive or relaxational) mode. Interestingly, the "underdamped DHO" option was always privileged by the algorithm over the "overdamped DHO" one, except for the highest Q spectra, namely for $Q \geq 13{,}55 nm^{-1}$. At these Q values, the posterior distributions of the low-frequency mode parameters unambiguously assessed the likelihood of its non-propagating character.

The ability of the used model to capture all relevant features of measured spectra supported *a posteriori* the implementation of the model in Equation 1, whose intrinsic simplicity minimizes the risk of an over-parametrization, further empowering the "Occam's razor" [40] (see also Chapter 28 of Ref. [41]) inherent to Bayesian inferential methods. A similar procedure was carried out on the dry sample as well: although the limited statistical accuracy prevents a reliable outcome for $\mathbf{Q}_{\parallel}$ spectra, the analysis of $\mathbf{Q}_{\perp}$ spectra indicates the presence of distinct inelastic modes. Figure 4 summarizes the overall scenario emerging from the Bayesian analysis by showing the Q dependence of the parameter Ω inferred for the various samples and geometries considered. It can be noticed therein that all dispersion curves belong to either of the following three branches:

1) An optical-like high-energy branch, only visible in a limited Q range. Notice that, although two highest Q points of this branch do not correspond to the highest probability posterior, they are included in the plot as consistent with the lower Q data.
2) A strongly Q-dispersive intermediate-energy branch.
3) Finally, a moderately Q-dispersive low-energy mode, only observable in the $\mathbf{Q}_{\perp}$ spectrum from the hydrated sample, and for Q larger than 6 nm^{-1}.

The first two branches do not have clear counterparts in the well-known spectral features of bulk water; furthermore, the second one is also visible in the dry sample. Finally, the damping Γ of these two excitations is relatively narrow, compatibly with a solid-like nature of the corresponding modes. All these facts support the assignment of the two higher energy branches to phonon excitations of the carbon matrix, the only solid-phase portion of our sample, considering that any sizable contribution from ice is to be excluded based on our diffraction measurements.

In Figure 4, the first two higher energy branches are respectively compared to the dispersion of the acoustic (black dashed line) and optic (red dashed line) phonon branches measured in Refs. [25] and [26] along the Γ-A direction (orthogonal to the graphene layers). These curves are reported after a rescaling of the Q-axis, which places the edge of the Brillouin zone at π/d_W = 7.85 nm^{-1}, where d_W is the inter-wall distance deduced from present diffraction measurements (~ 0.4 nm). Furthermore, the third, low-energy branch is compared to the dispersion curve of the transverse acoustic mode of water.[42]

In the following, we discuss in further detail the physical origin of the modes associated with these dispersion branches:

a) The two higher energy branches

The high-energy optical branch reported in Figure 4 relates to feeble features in the $\mathbf{Q}_\perp$ spectrum of the hydrated sample, and the posterior probability associated with the corresponding model DHO terms is thus extremely low. However, this dispersion branch reasonably agrees with the one of the optic phonon of graphite along the out-of-plane ($\Gamma \rightarrow$ A) direction (red dashed lines in Figure 4), measured in the IXS work of Ref. [25], which essentially confirmed previous INS measurements on pyrolytic graphite.[26] We thus assign this mode to optical-like vibration of the carbon matrix. The reason why this phonon mode could not be identified in the dry sample spectra likely stems from their limited statistical accuracy.

The highly dispersive intermediate energy mode can also be unambiguously assigned to the dynamics of the carbon matrix, due to both its presence in the dry sample spectrum and its consistency with the mentioned phonon dispersion of graphite (black dashed line in Figure 5).

The INS results were also interpreted by means of ab initio calculations on few-layer graphite [43] assigning the acoustic branch reported in Figure 4 to a breathing-like phonon mode of graphene layers; for MWCNTs, this mode should correspond to the expansion/contraction of the nanotube radius. This phonon branch is observed both in $\mathbf{Q}_\perp$ and $\mathbf{Q}_\parallel$ spectra, since, due to the closed character of the cylindrical surface, the carbon vibrations have a non-vanishing projection in both directions. While considering the analogy with few-layer graphene, the transition from planar to cylindrical geometry has two main consequences: 1) the breathing mode acquires a non-vanishing $Q = 0$ energy, *i.e.* it becomes optical rather than acoustic;[24] 2) When Q lays in the CNTs radial plane, as in the $\mathbf{Q}_\perp$ geometry, phonon modes of CNT are a linear combination of in-plane and out-of-plane movements of graphene carbons.[20] This implies that, in principle, both phonon types should be observable in IXS measurements on CNTs, and not only the out-of-plane (A→Γ) branch reported in Figure 4. However, in-plane graphene modes have energies well above the range typically covered by present IXS spectra,[24] thus not being a useful reference for current measurements.

b) The low-energy branch

The low-energy mode dominating the $\mathbf{Q}_\perp$ spectra can be assigned without ambiguities to collective modes of water, in view of its absence in the dry matrix, and it can be tentatively connected to the low-energy transverse mode. Notice that, in principle, transverse excitations are not detectable in the spectrum of density fluctuations at Q's corresponding to the first Brillouin zone of the crystal unless a coupling between longitudinal and transverse dynamics occurs,[15] as observed in several disordered systems.[44] Assigning this mode to the transverse dynamics of water would imply that aligned CNT arrays can filter the transverse polarization of phonon-like excitations of water molecules trapped in their interior.

Additional measurements

As discussed, one of the relevant conclusions of the presented work is that the spectral response of our sample is drastically different in the two considered geometries. In particular, it seems that the $\mathbf{Q}_{\parallel}$ spectra (see Figure 2) bear no evidence for any of the intense inelastic features which are known to dominate the spectrum of bulk water. Based on the evidence at hand, we cannot *a priori* exclude that this surprising behavior may be due to the limited amount of trapped water in the region illuminated by the incident X-Ray beam while performing $\mathbf{Q}_{\parallel}$ measurements, and that the prevalently elastic spectral profile may contain a significant spurious contribution from the aMWCNTs surroundings, i.e. from the thin substrate and the vertical aluminium holder it was glued on.

To clarify this point, we performed additional IXS measurements of $\mathbf{Q}_{\parallel}$ spectra on a sample with a higher hydration level, while holding the substrate vertical by means of a clamp sitting well out of the incident beam trajectory. In this sample the amount of confined water was increased by performing multiple autoclave cycles, as also confirmed *a posteriori* by measuring the $\mathbf{Q}_{\parallel}$ diffraction profile of the hydrated sample, whose difference from its dry sample counterpart was neat, as discussed further below.

The additional IXS measurements were carried out using the new IXS spectrometer at 10ID beamline of the NSLS II synchrotron source at Brookhaven National Laboratory. The IXS spectra measured at three Q values are reported in the left plot of Figure 5, and therein compared to: 1) the resolution profiles, and 2) for the two lowest Q's, to IXS spectra of bulk water

measured with the same spectrometer. For the sake of comparison, all curves are normalized to their maximum intensity.

Again, the left plot emphasizes that $\mathbf{Q}_{\parallel}$ spectra from the hydrated sample bear no evidence of the prominent longitudinal acoustic excitations dominating the inelastic portion of the bulk water spectrum; this reasonably confirms that likely the contribution from confined water to the $\mathbf{Q}_{\parallel}$ spectrum is mainly elastic.

The right plot of Figure 5 compares the diffraction profiles measured in the hydrated and dry samples in $\mathbf{Q}_{\parallel}$ geometry. These measurements were carried out using Grazing Incidence Wide-Angle X-Ray Scattering (GIWAXS) techniques at the CMS beamline of NSLS-II. In this case the $\mathbf{Q}_{\parallel}$ signal can be derived directly by looking at the intensity profile detected along a vertical strip of the 2D detector. Although the number and positions of relevant features in the diffraction profiles are essentially the same, it can be readily noticed that, upon hydration, the diffraction peak at about 18 nm^{-1} becomes considerably sharper. We finally remark that the diffraction profile of the wet sample bears no evidence of the features typically observed in bulk water.[45]

To exclude the possibility that a dry spot of the sample may have been illuminated by the beam in these $Q_{\parallel}$ measurements, additional diffraction measurements were performed on a wet and a dry sample. In these tests, several sample spots were illuminated by the beam. The comparison of various diffraction profiles of wet and dry samples suggests excluding the presence of dry spots in the wet sample. The results of this test are discussed in Supplemental Material (see also Fig. S3 therein).

Summarising, presented results urge us to conclude that the sample was properly hydrated and its spectra were, in both geometries, substantially different from the bulk water spectrum; this demonstrate that interstitial water contributed substantially to measured scattering signal, and that it was not bulk, as also suggested by the absence of phonon and Bragg peaks of ice respectively in the spectrum and diffraction pattern of the wet sample at 100 K.

We finally notice that an accurate subtraction of the carbon matrix signal from the wet sample spectrum would enable a more rigorous assessment of the interstitial water contribution. Unfortunately, this procedure would also require an absolute unit determination of the scattering profiles involved, which is hardly achievable on a rigorous basis, given the lack of knowledge on the amount of water trapped and its distribution throughout the forest. However, we can anticipate that this treatment would have little impact on the main conclusions of the presented analysis. In fact, the scattering of interstitial water clearly emerges in the wet sample's $Q_{\perp}$ spectrum, but not in the $Q_{\parallel}$ one, and not even on a logarithmic scale (see, e.g., Fig. 5). This implies that the carbon matrix signal, prevalently elastic in both geometries, does not obscure the inelastic contribution from trapped water, whose dependence on the scattering geometry reveals a clearly anisotropic nature.

CONCLUSION

We have discussed here the results of Inelastic X-ray Scattering (IXS) measurements on hydrated highly-oriented multi-walled aligned carbon nanotubes (aCNTs) "forest-grown" on a Si substrate. The measurements probed the dynamic response of the sample with a momentum transferred either orthogonally or longitudinally to the CNTs axis, the two scattering geometries being here labelled as $\mathbf{Q}_{\perp}$ and $\mathbf{Q}_{\parallel}$, respectively. The measured lineshapes demonstrate that the

dynamics of density fluctuations of axially confined water is, as expected, strongly anisotropic. Perhaps even more interestingly, while the $\mathbf{Q}_\perp$ spectrum of the hydrated sample is dominated by a low-energy inelastic feature, which we relate to a collective mode of confined water, no signatures of water collective dynamics were found in the $\mathbf{Q}_\parallel$ spectrum. Most importantly, the comparison with the literature suggests a direct link between the dominant $\mathbf{Q}_\perp$ mode mentioned above and the transverse acoustic mode of bulk water.[41] It may be thus tempting to conclude that carbon nanotube forests can be used to shape acoustic excitations propagating in water trapped therein, alternatively acting as "polarization filters" ($\mathbf{Q}_\perp$ geometry) or as "acoustic dampers" ($\mathbf{Q}_\parallel$ geometry) for these excitations. Although this conclusion may appear suggestive, it should still be considered that, at these terahertz frequencies and at mesoscopic scales, the polarization of acoustic modes propagating in a disordered material becomes somewhat ill-defined.

The other noticeable outcome of these measurements is a direct experimental observation of phonon modes in multi-walled CNTs, which we relate to those of graphite. As a natural extension of this study, the effect of highly directional confinement can be studied for non-associated, Van der Waals fluids, thus possibly assessing the universal nature of the observed confinement effects.

Acknowledgements

This work used resources of the National Synchrotron Light Source II, a U.S. Department of Energy (DOE) Office of Science User Facility operated for the DOE Office of Science by Brookhaven National Laboratory under Contract No. DE-SC0012704.

Author Contributions Statement

AC, ADF FF and MM designed the research, AC, YQC, AS and AA performed the IXS measurements, while AC and RL carried out diffraction ones; ADF and LS performed the Bayesian analysis; AC, AP and FDL took care of sample preparation; AC, ADF, FF and AP wrote the manuscript, which was then critically revised, commented and approved by all authors.

Additional information

The authors declare no competing interests.

References

[1] M. Maldovan, Sound and Heat Revolutions in Phononics, *Nature* **503,** 209 (2013).

[2] R. Saito, G. Dresselhaus, M. S. Dresselhaus, *Physical Properties of Carbon Nanotubes*, World Scientific*,* (1998).

[3] B. Mukherjee, P. K. Maiti, C. Dasgupta, A. Sood, Single-File Diffusion of Water Inside Narrow Carbon Nanorings, *ACS Nano* **4***,* 985 (2010).

[4] J. Köfinger, G. Hummer, C. Dellago, Macroscopically Ordered Water in Nanopores, *Proc. Natl. Acad. Sci. U.S.A.* **105***,* 13218 (2008).

[5] C. Cametti, F. De Luca, A. Parmentier, Radiowave Dielectric Investigation of Water Confined in Channels of Carbon Nanotubes, *J. Chem. Phys.* **137***,* 094908 (2012).

[6] B. Mukherjee, P. K. Maiti, C. Dasgupta, A. K. Sood, Strongly Anisotropic Orientational Relaxation of Water Molecules in Narrow Carbon Nanotubes and Nanorings, *ACS Nano* **2***,* 1189 (2008).

[7] E. Mamontov, C. Burnham, S.-H. Chen, A. Moravsky, C.-K. Loong, N. De Souza, A. Kolesnikov, Dynamics of Water Confined in Single–And Double-Wall Carbon Nanotubes, *J. Chem. Phys.* **124***,* 194703 (2006).

[8] A. I. Kolesnikov, J.M. Zanotti, C.K. Loong,, P. Thiyagarajan, A. P. Moravsky, R. O. Loutfy, C. J. Burnham, Anomalously Soft Dynamics of Water in a Nanotube: A Revelation of Nanoscale Confinement, *Phys. Rev. Lett.* **93***,* 035503 (2004).

[9] G. Briganti, G. Rogati, A. Parmentier, M. Maccarini, F. De Luca, Neutron Scattering Observation of Quasi-Free Rotations of Water Confined in Carbon Nanotubes, *Sci. Rep.* **7***,* 45021 (2017).

[10] S. Vaitheeswaran, J. C. Rasaiah, G. Hummer, Electric Field and Temperature Effects on Water in the Narrow Nonpolar Pores of Carbon Nanotubes, *J. Chem. Phys.* **121***,* 7955 (2004).

[11] M.H. Koehler, J. R. Bordin, L. B. da Silva, M. Barbosa, Structure and Dynamics of Water Inside Hydrophobic and Hydrophilic Nanotubes, *Physica A* **490**, 331 (2018).

[12] A. Striolo, The Mechanism of Water Diffusion in Narrow Carbon Nanotubes, *Nano Lett.* **6***,* 633 (2006).

[13] Y.-G. Zheng, H.-F. Ye, Z.-Q. Zhang, H.-W Zhang, Water Diffusion Inside Carbon Nanotubes: Mutual Effects of Surface and Confinement, *Phys. Chem. Chem. Phys.* **14***,* 964 (2012).

[14] M. Sampoli, G. Ruocco, F. Sette, Mixing of Longitudinal and Transverse Dynamics in Liquid Water, *Phys. Rev. Lett.* **79***,* 1678 (1997).

[15] E. Pontecorvo, M. Krisch, A. Cunsolo, G. Monaco, A. Mermet, R. Verbeni, F. Sette, G. Ruocco, High-Frequency Longitudinal and Transverse Dynamics in Water, *Phys. Rev. E* **71***,* 011501 (2005).

[16] A. Cunsolo, The THz Spectrum of Density Fluctuations of Water: The Viscoelastic Regime, *Adv. Cond. Matter Phys.* **2015**, 137435 (2015).

[17] A. Cimatoribus, S. Saccani, F. Bencivenga, A. Gessini, M. G. Izzo, C. Masciovecchio, The Mixed Longitudinal–Transverse Nature of Collective Modes in Water, *New J. Phys.* **12**, 053008 (2010).

[18] G. E.Walrafen, Raman Spectral Studies of the Effects of Temperature on Water and Electrolyte Solutions, *J. Chem Phys.* **44***,* 1546 (1966).

[19] O. V. Kharissova, B. I. Kharisov, Variations of Interlayer Spacing in Carbon Nanotubes, *RSC Adv.* **4***,* 30807 (2014).

[20] S. K. Sinha, Theory of Inelastic X-Ray Scattering From Condensed Matter, *J. Phys. Condens. Matter* **13***,* 7511 (2001).

[21] S. W. Lovesey, *Theory of Neutron Scattering from Condensed Matter,* Clarendon Press: Oxford Vol. 1, (1984).

[22] Z. Zhou, T. Gao, S. McCarthy, A. Kozbial, S. Tan, D. Pekker, L. Li, P. W. Leu, Parahydrophobicity and Stick-Slip Wetting Dynamics of Vertically Aligned Carbon Nanotube Forests, *Carbon* **152**, 474 (2019).

[23] See Supplemental Material at […] for a discussion of diffraction and inelastic scattering measurements at 100 K, a succinct report on test diffraction measurements, a microscopy image of the sample, and further details on the Bayesian inference analysis.

[24] M. Dresselhaus, P. Eklund, Phonons in Carbon Nanotubes, *Adv. Phys.* **49**, 705 (2000).

[25] M. Mohr, J. Maultzsch, E. Dobardžic, S. Reich, I. Miloševic, M. Damnjanovic, A. Bosak, M. Krisch, C. Thomsen, Phonon Dispersion of Graphite by Inelastic X-Ray Scattering, *Phys. Rev.* B **76***,* 035439 (2007).

[26] R. Nicklow, N. Wakabayashi, H. Smith, Lattice Dynamics of Pyrolytic Graphite, *Phys. Rev. B* **5***,* 4951 (1972).

[27] M. Bayes, M. Price, An Essay towards Solving a Problem in the Doctrine of Chances. By the Late Rev. Mr. Bayes, FRS Communicated by Mr. Price, in a Letter to John Canton, *AMFRS. Phil. Trans.* (1683-1775) 370-418, **1763**.

[28] P. J. Green, Reversible Jump Markov Chain Monte Carlo Computation and Bayesian Model Determination, *Biometrika* **82***,* 711 (1995).

[29] A. H. Said, H. Sinn, R. Divan,New Developments in Fabrication of High-Energy-Resolution Analyzers for Inelastic X-Ray Spectroscopy, *J. Synchrotron Radiat.* **18,** 492 (2011).

[30] T. S. Toellner, A. Alatas, A. H. Said, Six-Reflection meV-Monochromator for Synchrotron Radiation, *J. Synchrotron Radiat.* **18***,* 605 (2011).

[31] Y. Q. Cai, D. S. Coburn, A. Cunsolo, J. W. Keister, M. G. Honnicke, X.R. Huang, C. N. Kodituwakku, Y. Stetsko, A. Suvorov, N. Hiraoka, K. D. Tsuei, H. C. Wille, The Ultrahigh

Resolution IXS Beamline of NSLS-II: Recent Advances and Scientific Opportunities, *J. Phys. Conf. Ser.* **425**, 202001 (2013).

[32] M. Yabashi, K. Tamasaku, S. Kikuta, T. Ishikawa, X-Ray Monochromator With an Energy Resolution of $8x10^9$ at 14.41 keV, *Rev. Sci. Inst.* **72**, 4080 (2001).

[33] G. Reiter, C. Burnham, D. Homouz, P. Platzman, J. Mayers, T. Abdul-Redah, A. Moravsky, J. Li, C.-K. Loong, A. Kolesnikov, Anomalous Behavior of Proton Zero Point Motion in Water Confined in Carbon Nanotubes, *Phys. Rev. Lett.* **97**, 247801 (2006).

[34] A. De Francesco, E. Guarini, U. Bafile, F. Formisano, L. Scaccia, Bayesian Approach to the Analysis of Neutron Brillouin Scattering Data on Liquid Metals, *Phys. Rev. E* **94**, 023305 (2016).

[35] A. De Francesco, L. Scaccia, M. Maccarini, F. Formisano, Y. Zhang, O. Gang, D. Nykypanchuk, A. H. Said, B. M. Leu, A. Alatas, Damping Off Terahertz Sound Modes of a Liquid upon Immersion of Nanoparticles, *ACS Nano* **12**, 8867 (2018).

[36] H. Mori, A continued-fraction representation of the time-correlation functions, *Prog. Theor. Phys.* **34**, *3*99 (1965).

[37] R. Zwanzig,, Experimental Determination of the Structural Relaxation in Liquid Water, *J. Chem. Phys*. **43**, 714 (1965).

[38] A. Cunsolo, G. Ruocco, F. Sette, C. Masciovecchio, A. Mermet, G. Monaco, M. Sampoli, R. Verbeni, Experimental Determination of the Structural Relaxation in Liquid Water, *Phys. Rev. Lett.* **82**, 775 (1999).

[39] G. Monaco, A. Cunsolo, G. Ruocco, F. Sette, *Phys. Rev. E* **60**, Viscoelastic Behavior of Water in the Terahertz-Frequency Range: An Inelastic X-Ray Scattering Study, 5505 (1999).

[40] J. O. Berger, W. H. Jefferys, *J. It. Stat. Soc.* **1**, 17 (1992).

[41] D.J. MacKay, *Information Theory, Inferential and Learning Algorithms*, Cambridge University Press. (2003)

[42] A. Cunsolo, C. N. Kodituwakku, F. Bencivenga, M. Frontzek, B. M. Leu, A. H. Said, Transverse Dynamics of Water Across the Melting Point: A Parallel Neutron and X-Ray Inelastic Scattering Study, *Phys. Rev. B* **85**, 174305 (2012).

[43] J.W. Jiang, H. Tang, B.S. Wang, Z.B. Su, Raman and Infrared Properties and Layer Dependence of the Phonon Dispersions in Multilayered Graphene, *Phys. Rev. B* **77***,* 235421 (2008).

[44] A. Cunsolo, A. Suvorov, Y. Q. Cai, The Onset of Shear Modes in the High Frequency Spectrum of Simple Disordered Systems: Current Knowledge and Perspectives, *Phil. Mag.* **96***,* 732 (2016).

[45] C. Huang, K. T. Wikfeldt, D. Nordlund, U. Bergmann, T. McQueen, J. Sellberg, L. G. M. Pettersson, A. Nilsson, Wide-Angle X-Ray Diffraction and Molecular Dynamics Study of Medium-Range Order in Ambient and Hot Water, *Phys. Chem. Chem. Phys.* **13**, 19997 (2011).

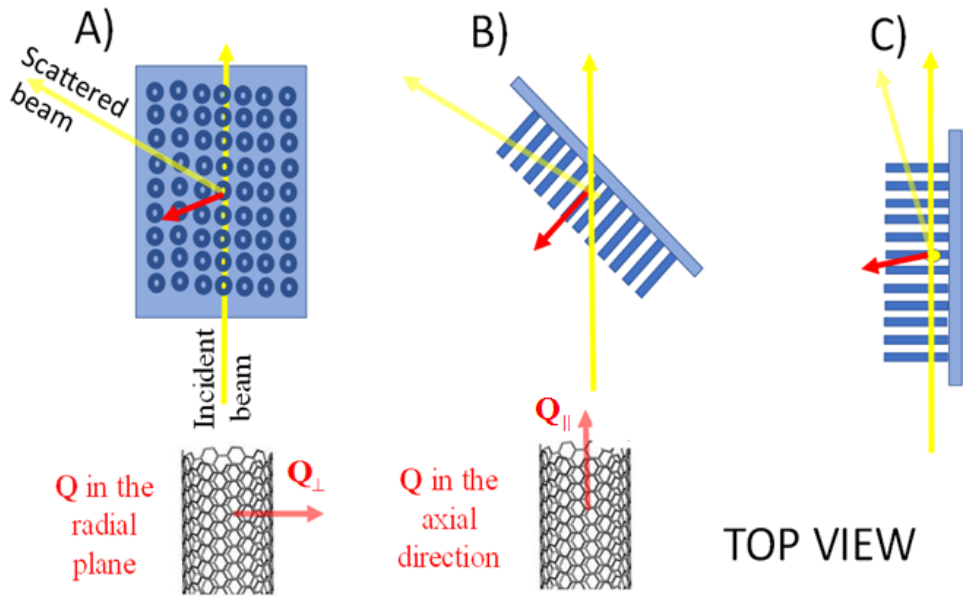

Figure 1: *Sketches illustrating the experimental scattering geometries used to detect collective modes that exchange momentum either orthogonal (*$\mathbf{Q}_\perp$*, case A) or parallel (*$\mathbf{Q}_\parallel$*, case B), as discussed in the text. Notice that the switch between* $\mathbf{Q}_\perp$ *and* $\mathbf{Q}_\parallel$ *geometries is implemented by rotating the substrate from a position parallel to the scattering plane to one orthogonal to it. Panel (C) illustrates the grazing geometry actually adopted for the* $\mathbf{Q}_\parallel$ *measurements (see text).*

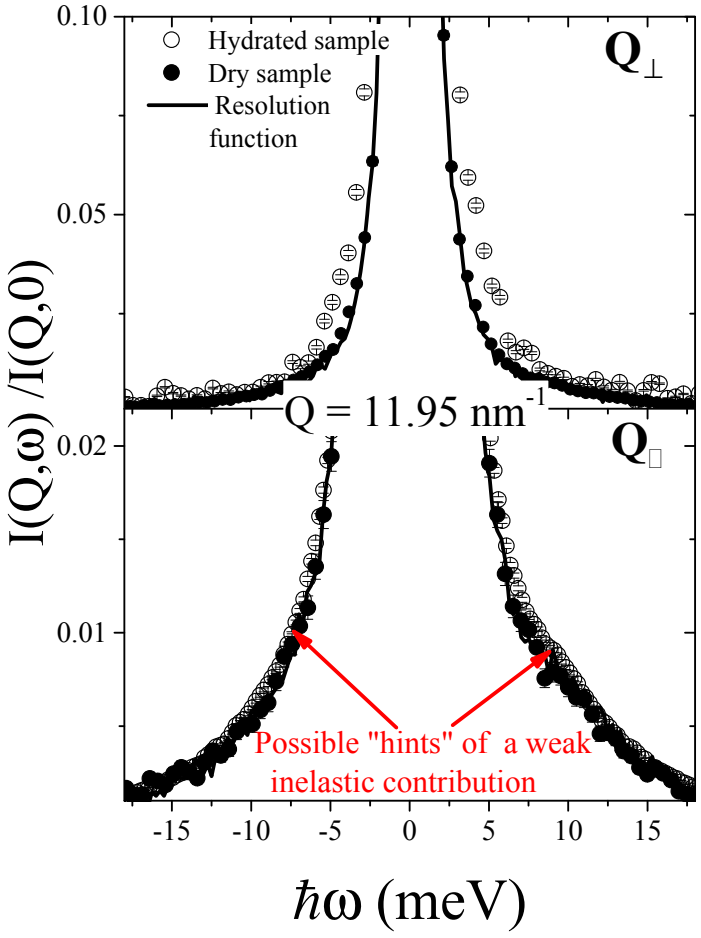

Figure 2: *Comparison between the IXS spectra measured at Q = 11.95 nm^{-1} on the dry and the hydrated sample (full and empty dots respectively) in the two scattering geometries. Data are normalized to the maximum intensity and compared to the correspondingly normalized instrumental resolution profiles (solid lines). The possible presence of a weak inelastic feature in the* $\mathbf{Q}_{\parallel}$ *spectra is evidenced by the arrows in the plot. Notice that the error bars are within the symbol sizes for all IXS spectra except the one from the dry sample in the* $\mathbf{Q}_{\parallel}$ *geometry.*

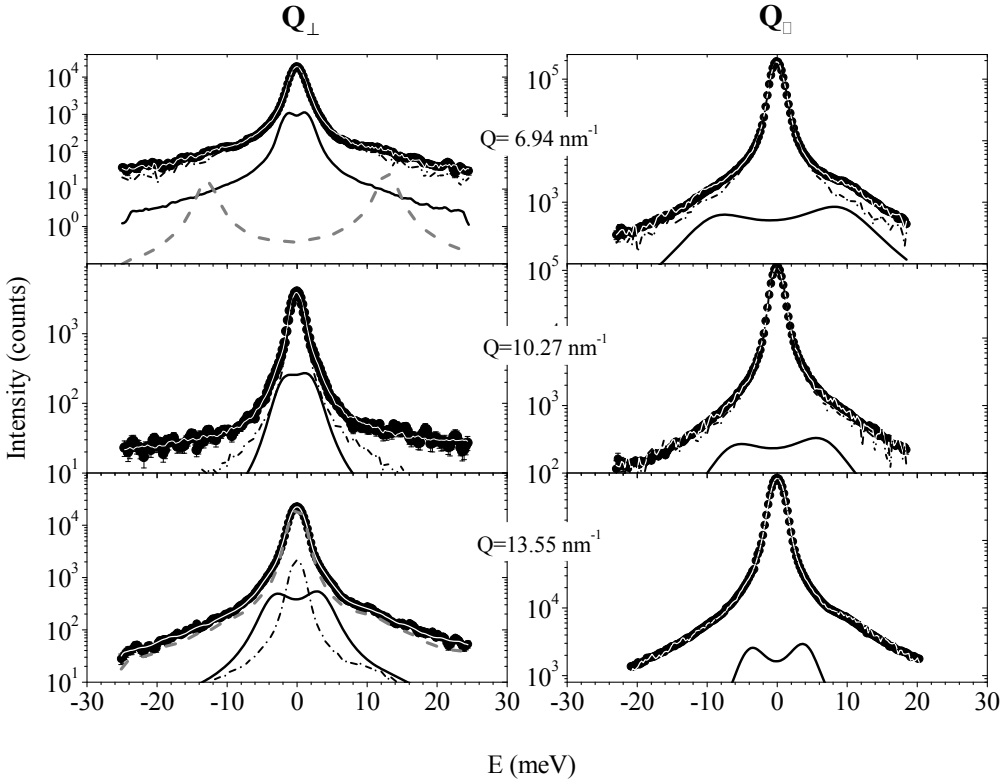

Figure 3: *IXS spectra of the hydrated aMWCNTs at ambient condition are reported as measured at the Q values indicated in the plots in the* $\mathbf{Q}_\perp$ *(left column) and* $\mathbf{Q}_\parallel$ *(right column) scattering geometries. In both geometries, the raw data (dots) are compared to best-fitting model lineshapes (white lines through data), along with the elastic (dash-dotted line), plus a first inelastic DHO term (thick line). Notice that, for the Q = 6.94 nm^{-1} and 13.55 nm^{-1}* $\mathbf{Q}_\perp$ *spectra, the most probable models include an additional DHO, reported as a grey dashed line, and respectively describing either an inelastic excitation or a quasielastic one.*

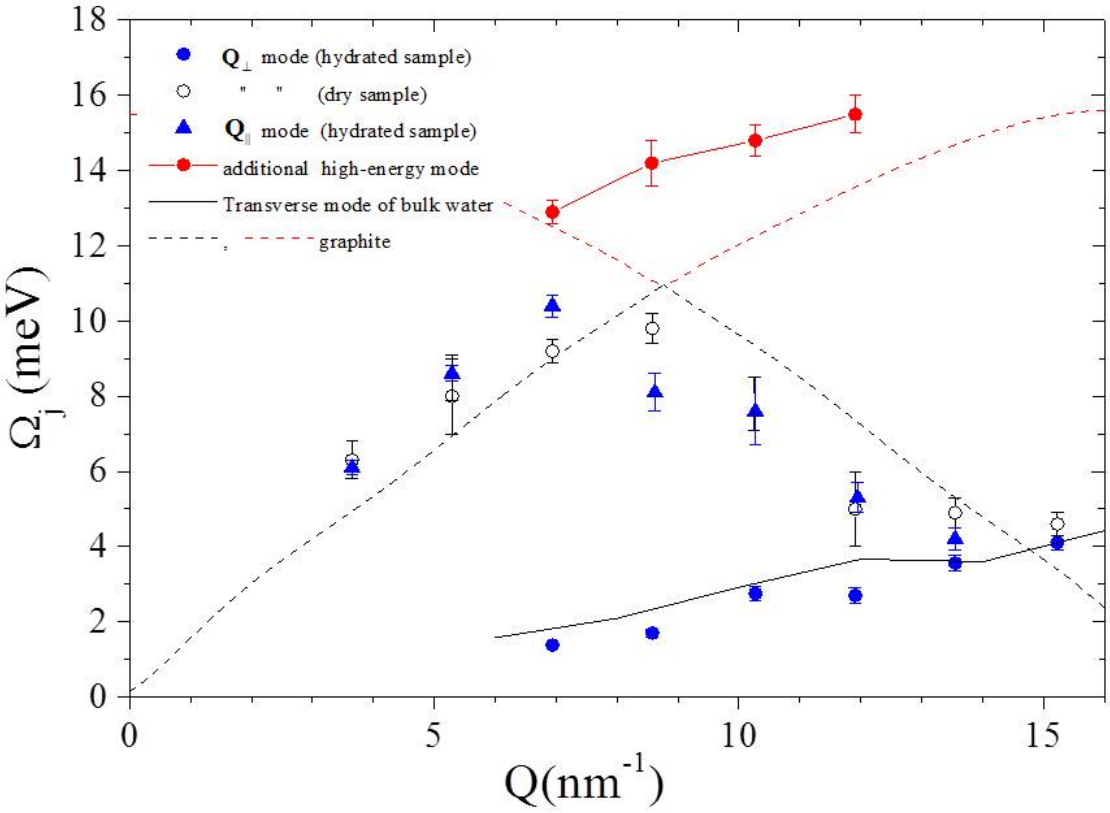

Figure 4: *Dispersion curves derived for the aMWCNTs sample in the dry and hydrated samples, for both* $\mathbf{Q}_{\perp}$ *and* $\mathbf{Q}_{\parallel}$ *scattering geometries (see legend). The dispersion curves of bulk water and graphite are also included as derived from Ref.* [36] *and Ref.* [24]*, respectively. The presence of the additional high-energy mode is suggested by the algorithm, although with a low plausibility at the two highest Q's (see text).*

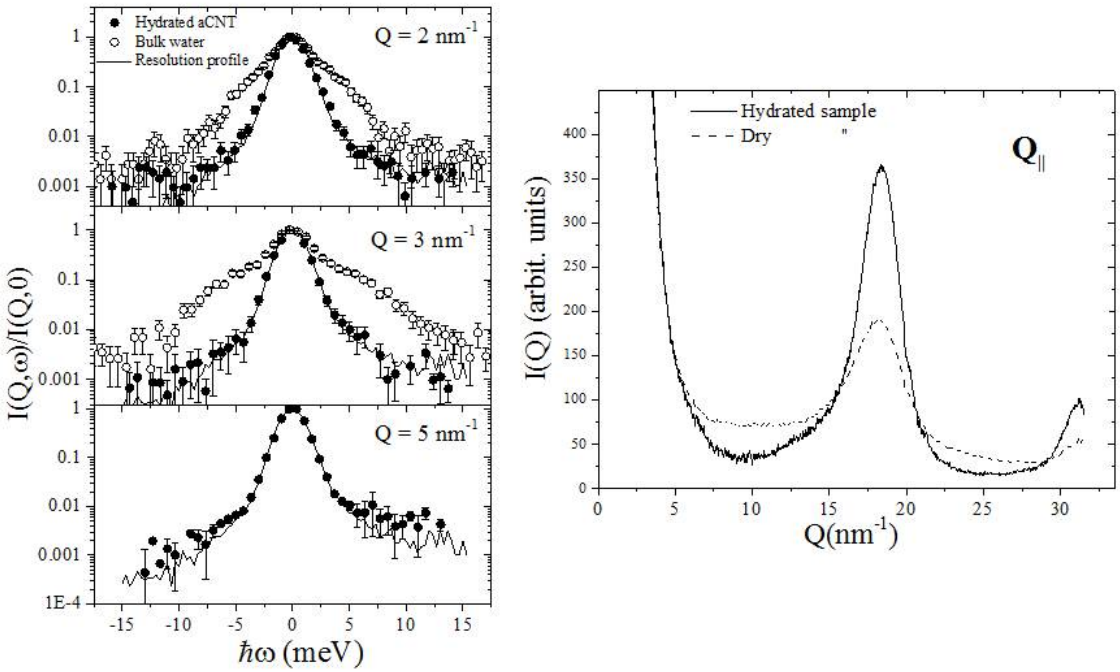

Figure 5: *Left Panel: IXS spectral shapes in* $\mathbf{Q}_{\parallel}$ *geometry from the hydrated aCNT sample and bulk water with respect to the resolution profile (measurements from 10ID spectrometer at NSLS II facility). Right Panel: Grazing Incidence Wide Angle Scattering (GIWAXS) profiles from the dry and the hydrated samples are compared to each other (measurements from the 11BM beamline at NSLS II facility).*